Chapter 2
Functional Properties of Polydomain Ferroelectric Oxide Thin Films

E.P. Houwman, K. Vergeer, G. Koster and G. Rijnders

Abstract The properties of a ferroelectric, (001)-oriented, thin film clamped to a substrate are investigated analytically and numerically. The emphasis is on the tetragonal, polydomain, ferroelectric phase, using a three domain structure, as is observed experimentally, instead of the two-domain structure used in earlier literature. The previously used, very restrictive set of boundary conditions, arising from the domain walls, is relaxed, creating more modes for energy relaxation. It is argued that this approach gives a more realistic description of the clamped ferroelectric film. It is shown that for the ferroelectric oxides $PbZr_{1-x}Ti_xO_3$, the tetragonal, polydomain phase is present over a wide range of substrate induced strains for $x \geq 0.5$, corresponding to the tetragonal side of the bulk phase diagram. A polydomain, rhombohedral phase is present for $x < 0.5$, at the bulk rhombohedral side. Phase-temperature diagrams, and ferroelectric, dielectric, and piezoelectric properties as well as lattice parameters are calculated as function of substrate induced strain and applied field. The analytical formulation allows the decomposition of the numerically obtained values of these properties into three different causes: domain wall motion, field induced elastic effects, and piezoelectric effects. It is found that domain wall motion and polarization rotation of the in-plane oriented domains under an applied field contribute most to the properties, while the out-of-plane oriented domains hardly contribute.

Keywords Ferroelectrics · Polydomain · Landau-Devonshire theory · PZT · Thin film

E.P. Houwman (✉) · K. Vergeer · G. Koster · G. Rijnders
Inorganic Material Science, MESA+ Institute of Nanotechnology, University of Twente, Enschede, The Netherlands
e-mail: e.p.houwman@utwente.nl

K. Vergeer
Materials Innovation Institute (M2i), Delft, The Netherlands

H. Nishikawa et al. (eds.), *Correlated Functional Oxides*
DOI 10.1007/978-3-319-43779-8_2

2.1 Introduction

Complex oxides and specifically the class of the perovskites have been investigated already for a long time for their broad range of physical properties [2, 4, 15, 19]. More recently also perovskite thin films have become of interest, kick started by the arrival of the high temperature superconductors around 1990. Although many interesting perovskites have been investigated practical applications are still rare. However, the group of perovskite ferroelectric and piezoelectric materials and notably the solid solution group $PbZr_{1-x}Ti_xO_3$ (or short PZT), which shows the strongest ferro/piezoelectric properties up to relatively high temperatures, is already applied extensively, also in thin film applications. In bulk, the most used composition is that of the morphotropic phase boundary (MPB) for $x \approx 0.48$, between the tetragonal phase ($x > 0.48$), and the rhombohedral phase ($x < 0.48$) at room temperature. Despite the long history of research into ferro/piezoelectric materials and the thorough understanding of the basic mechanisms in these materials it is in practice hard to describe the properties of PZT (or any other ferro/piezoelectric material) in real devices quantitatively very accurately, due to the large number of extrinsic effects that can play a role.

Ferro/piezoelectric thin films are of great interest for memory devices and in MEMS applications because of their promise of miniaturization of mechanical devices. In both cases, the integration of the perovskite crystal structure with different electrode and substrate (especially with Si) crystal structures is of utmost importance. On the other hand for studying the intrinsic effects one mostly uses perovskite substrates. There is a long list of design variables that influence the properties of the thin film, such as the choice of (a) the substrate—single or polycrystalline or even amorphous (glass)—determining to a large extent the crystal growth. (b) Additional buffer layers between the substrate and the ferroelectric film may alleviate possible lattice mismatches [3], while oxide nanosheets can allow coherent growth on amorphous substrates [1]. (c) The choice of the bottom electrode material, which may also act as a buffer layer, determines to a large extend the initial growth layer of the functional ferroelectric layer. This can cause several interface related electrical effects such as voltage self-bias of the device, domain wall pinning, affecting the coercive field, and surface passive layers. Furthermore, these effects may depend on time through the field cycling of the device, causing aging of the device properties, due to diffusion of charges, and ions between electrode and functional layer. (d) The substrate/buffer layer stack in most cases dictates the growth orientation of the functional layer [3], which in turn may affect device properties, especially when the polarization axis is strongly coupled to the crystal structure, as is the case for compositions away from the MPB. (e) The higher the in-plane alignment of the crystal structure of the individual grains in the film, the less effect the grain boundaries on the film properties is observed and the highest ferroelectric properties, even without electrical poling [6]. Such devices appear not to suffer from aging effects, a property that is very important for many applications. (f) Although experimentalists tend to choose the MPB composition when aiming

for the largest piezoelectric coefficients, it is far from clear that this is the right choice for PZT thin films. For example it was observed that (110)-oriented PZT on Si has the highest piezoelectric coefficient e_{31} for $x \approx 0.6$ and not for 0.48 [18]. (g) Finally, we want to mention the important role of the ferroelectric domain structure in the properties of ferro/piezoelectrics [17]. This is well known in bulk single crystal devices, where one engineers the domain structure to optimize device properties by using specific crystal cuts. However, this is still a field in its infancy for thin film devices. But with the increasing control over thin film growth one may also envision the design of domain structures in thin film devices.

With the advent of high quality PZT thin films there has been much theoretical development in understanding many of the extrinsic effects, which have been summarized in the review book of Tagantsev et al. [17]. As seen above many effects are related to the crystalline quality of the grown films. In practice it is not straightforward to separate extrinsic effects from the intrinsic properties of the thin film, because the latter are affected by the film clamping. However, in well defined situations it is possible to model the modified properties of clamped ferro/piezoelectric thin films. Thus if such a model is available, one can make a better effort to separate other extrinsic effects, arising from for example grain boundaries, from that of the film clamping. This is of great importance for understanding thin film properties and the improvement of thin films applications.

In this chapter, we modify an earlier model in literature for describing the ferro/piezoelectric properties of a clamped ferroelectric, polydomain thin film [9, 10]. We reconsidered the ferroelectric domain structure, essentially going from a 1D to a 2D description and investigate the consequences for the film properties. The discussion is limited to about 0.5–2 μm thick PZT thin films usually needed in Si-based MEMS devices. Further the discussion is limited to (001)-oriented epitaxial films (no grain boundaries). We expect that the model is equally well applicable to other materials and can be modified in the future to other film orientations and more disordered films.

2.2 Polydomain Ferroelectric Thin Films

For understanding the relation between film properties and the above list of structural variables, models are needed that describe the dielectric, ferroelectric, and piezoelectric behavior of thin films. For piezoelectric applications, the film areas are generally much larger than typical ferroelectric domain sizes, thus an appropriate model should take into account the domain structure and its response to external forces, such as applied stresses or an applied electrical field. Ferroelectric domain formation in ferroelectric films driven by elastic constraints has been studied by various authors. Recently, Tagantsev et al. [17] summarized the various models existing in literature, which can be distinguished in three principal approaches. In the *mean-strain approach*, initiated by Roitburd [16], the average mechanical energy of the system is minimized by the creation of subdomains, without

considering the coupling to polarization. A second approach is based on the Landau theory of the dense domain structure [9, 10, 14] which takes into account the stress dependence of the order parameter (the polarization) by the piezoelectric effect. In the phase-field approach [11, 12] the polarization relaxes using time-dependent Ginzburg-Landau equations.

In this chapter, we reconsider the model of Pertsev and Koukhar for several reasons. In their model only a two-domain structure is considered, whereas the observed domain structure of tetragonal PZT thin films contains more domains. Specifically, the (001)-oriented tetragonal films show not only c/a, but also c/b-subdomain structures. (See Atomic Force Measurement in Fig. 2.1g). Further, we will argue that one can relax the very strict boundary conditions imposed by Pertsev and Koukhar. We take these aspects into account and model the consequences analytically as far as possible, as well as numerically. Secondly, in many cases engineering oriented experimentalists measure film properties as function of applied field rather than of temperature, as was mostly discussed in literature. Therefore, we also consider the effect of the applied field on the domain structure and ferroelectric and piezoelectric film properties. It is noted that the model is in principle static and does not account for the frequency dependence of domain wall motion, which may arise from the coupling of domain walls with crystalline defects and its effect on the device properties. The present model may be of help in separating the contributions from domain wall motion from those arising from the static, intrinsic contributions of the clamped film.

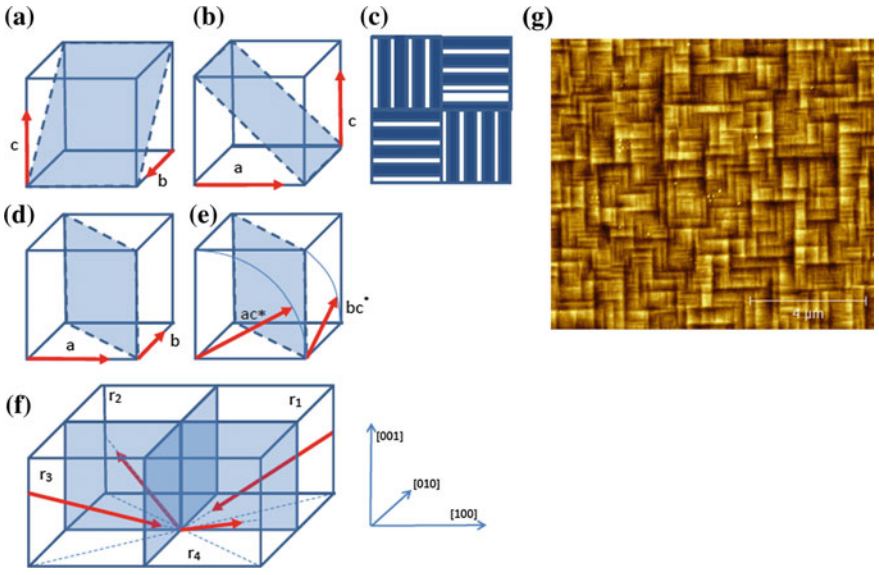

Fig. 2.1 Schematic domain substructures c/b (**a**) and c/a (**b**). Top view of *c*/*b*/*a* domain structure (**c**). *a*/*b* domain structure in zero (**d**) and finite field (**e**). *r*-phase structure (**f**). AFM picture of a PZT40/60 thin film (**g**)

The remainder of this chapter is structured as follows. In Sect. 2.3, we describe a clamped thin film and under which conditions one can simplify the description to a mathematically treatable problem, without losing the essential characteristics of a realistic thin film. In Sect 2.3.1 a general expression for the free energy of a polydomain, clamped thin film, and the boundary conditions are given. The analytical model is applied to the tetragonal phase in Sect. 2.3.2, and the properties of this phase are described in Sects. 2.3.3–2.3.5. In Sect. 2.4, the results of the numerical analysis of all phases are presented and these are interpreted in terms of the derived analytical descriptions. In Sect. 2.5 we summarize the main results.

2.3 Model of a Polydomain PZT Thin Film

We study thick, single-crystalline, epitaxial films (in this paper specifically made of PZT) grown in the paraelectric state at deposition temperature T_d on a thick substrate of a dissimilar material (specifically perovskites like $SrTiO_3$ (STO), $DyScO_3$ (DSO), and others, as well as Si, with appropriate buffer layers). For film thicknesses larger than a few 100 nm one can generally consider the bulk of the film to be fully relaxed at T_d due to the incorporation of growth defects in the initial growth layer, which resolves the epitaxial lattice mismatch between film and substrate (or eventual buffer or bottom electrode layer) at T_d. Since T_d is generally above the paraelectric–ferroelectric transition temperature T_C the PZT is in its cubic parent phase during deposition. The thickness of the initial growth layer is of the order of at most a few 10s of nm, which is of the order of a few percent of the thickness range of films normally used in piezoelectric applications, 500–2000 nm. During cool down, the film experiences tensile or compressive stress due to the difference in thermal expansion coefficients of the film and the substrate. It is assumed that the thick substrate does not deform. This is the so-called clamped film condition. The substrate induced thermal strain of a film at temperature T, that is strain-free at deposition temperature, can be shown to be

$$S_m(T) = \left(\frac{a_s^* - a_0}{a_0}\right)_T \approx \left(\alpha_f - \alpha_s\right)(T_\mathrm{d} - T) \tag{2.1}$$

Here α_f and α_s are the thermal expansion coefficients of the film and the substrate, respectively. $a_s^* = a_0(1 + S_m)$ and a_0 are respectively an effective substrate parameter and the pseudocubic lattice parameter of the film, both at the considered temperature T. Note that for a thick film this strain is imposed on the complete film, thus the average in-plane strains in the film must be equal to this value, whereas in a coherently grown epitaxial film, this strain is imposed to the individual unit cells of the film. The consequence of this is that a coherently grown film must always be in a single domain phase, because the coherence is lost when domain formation occurs. The experimentally accessible strain range by using different substrates is

defined by their thermal expansion coefficients. With $\alpha_f \approx 5-6$ ppm/K for PZT and $\alpha_s \approx 0-11$ ppm/K (0 for zero thermal expansion glass substrates using nanosheet buffer layers [1], 2.4 for Si up to 11 for STO) and usual $T_d = 600$ °C one obtains a fairly narrow accessible strain range, $S_m = -0.0032$ to 0.0032. One might slightly extend the range at the compressive side by using metal substrates, provided suitable buffer layers can be found. For larger (absolute) strain values one has in practice to resort to bending of substrates.

When the film is cooled down through the Curie temperature T_C, the thermal induced stress can be (partly) resolved by the formation of a ferroelastic domain structure, for example the well known c/a domain structure of a tetragonal PZT composition, consisting of alternating 45° inclined slabs of c and a domains. Another mechanism is rotation of the polarization vector in the domains, which changes the unit cell lattice parameters through the coupling between strain and polarization. As argued in literature [9] in relatively thick films the domain widths D are much smaller than the film thickness H, so that the polarization and strain fields within each domain can be considered to be homogeneous. Thus also the energy density in a polydomain epitaxial film is therefore piecewise homogeneous. Further it was argued that the energy contribution of the thin layers (thickness $h(\sim D) \ll H$) with inhomogeneous internal fields near the top and bottom interface, to the total free energy can be neglected. Kouhkar et al. [9] argue that the energy contribution of the domain wall self-energy is small under the condition $D \ll H$, which holds for thick films. One can relax this condition if one assumes that the domain wall energy per unit domain wall area γ is constant and that the total area of the domain walls does not change. As long as the phase does not change the domain wall positions only shift under varying mechanical or electrical field conditions and the total domain wall energy per unit volume should not change very much. In the following, we will see that in practice this is mostly the case. We consider a device structure with short-circuited or voltage-biased top and bottom electrodes and no internal charges, thus depolarization does not contribute to the total energy.

Before explaining the model assumptions we need to specify the concepts phase and domain more precisely. With the term 'phase' we indicate the crystallographic structure of the film. This can be a monodomain phase, such as the tetragonal c-phase or the cubic paraelectric p-phase, as well as a polydomain phase, with rhombohedral or tetragonal unit cells with different orientation of the long axis, such as the $r_1/r_2/r_3/r_4$, $c/b/a$, or the a/b phase. With a '*domain*', we indicate as usual the subvolumes within a phase with the same orientation of the unit cells. The polarization can still have different orientations for the same type of domains, for example P_1 and $-P_1$ in an a-domain. Table 2.1 gives the polarization vectors in each domain (in the pseudocubic lattice), the number of possible polarization orientations (with positive P_3), and the number of possible domains. In Fig. 2.1, the possible domain structures considered here are schematically shown using the pseudocubic representation of the (001)-oriented PZT unit cell.

Table 2.1 Polarization vectors, number of domains, and polarization orientations in a polydomain film and the number of different free energy functions in (2.4)

Phase	c	$c/b/a$	$c/bc^*/ac^*$	a/b	ac^*/bc^*	r	p
Polarization vectors							
'c'-type	$(0,0,P_c)$	$(0,0,P_c)$	$(0,0,P_c)$				$(0,0,0)$
'a'-type		$(P_a,0,0)$	$(P_a,0,P^*)$	$(P_a,0,0)$	$(P_a,0,P^*)$		
'b'-type		$(0,P_a,0)$	$(0,P_a,P^*)$	$(0,P_a,0)$	$(0,P_a,P^*)$		
'r'-type						(P_1,P_1,P_3)	
Domain fraction	$\phi_c = 1$	$\phi_a = \phi_b = \frac{1-\phi_c}{2}$	$\phi_{ac^*} = \phi_{\overline{ac^*}} = \phi_{bc^*} = \phi_{\overline{bc^*}} = \frac{1-\phi_c}{4}$	$\phi_a = \phi_b = 1/2$	$\phi_{ac^*} = \phi_{\overline{ac^*}} = \phi_{bc^*} = \phi_{\overline{bc^*}} = 1/4$	$\phi_{r_i} = 1/4$	$\phi_p = 1$
Domains	1	3	5	2	4	4	1
P-orient[a]	1	5	5	4	4	4	0
F-funct.	1	2	2	1	1	1	1

[a]The number of possible polarization orientations is doubled counting also the $-P_3$ vector components

The approach to obtain a description of the polydomain state, as is presented here, is different from that followed in literature in three aspects. It is necessary to discuss these differences since they give rise to significant qualitative and quantitative differences in the properties of the polydomain phases.

(1) There are several polydomain phases possible in the model, however, there is only one phase that gives rise to an additional parameter, that can be used to minimize the total energy. This is the domain volume fraction of c domains, $\phi = V_c/V_{\text{tot}}$ in the polydomain tetragonal phase. In literature, this phase is considered to consist of the c/a phase, build up from alternating domains of out-of-plane (c domains) and in-plane oriented domains in one direction (a domains), separated by 45° inclined {101} domain walls (see Fig. 2.1b). This one-dimensional (1D) problem description is assumed to be representative for the polydomain state of a 2D film. The consequence of this is that the strain and stress states of the domains are asymmetric in the two in-plane directions. *Here*, we explicitly consider the presence of both c/a and c/b domain structures in the film (Fig. 2.1a, b, c). For large tensile strains one expects all polarization vectors to be in the film plane to produce a two-domain a/b domain structure (Fig. 2.1d), with {110} domain walls. Under the influence of an out-of-plane electrical field, the polarization vectors will tilt out of the plane to give the ac^*/bc^* domain structure (Fig. 2.1e). For small c^* components one expects that these domains can be combined with c-domains in domain structures c/ac^* and c/bc^* similar to the c/a and c/b domains, to create a $c/bc^*/ac^*$ structure. Thus, although the basic crystal structure may be for example tetragonal, under the influence of stress or electrical fields, the crystal symmetry can change and the polarization orientation changes accordingly. The rhombohedral domain structure $r_1/r_2/r_3/r_4$ (in short the r-phase) (Fig. 2.1f) is expected to arise in the case of rhombohedral compositions. It is obvious that phase transitions between for example the $c/b/a$ phase and the r-phase require a large rearrangement of domain walls, whereas a change of domain fraction in the $c/b/a$ phase is a much less involved operation. On the other hand, the phase change from $c/b/a$ to the a/b or c phase goes gradually with a gradual change of the domain wall structure. It is clear that, since the model described here does not take into account domain wall energies, the model cannot treat possible energy barriers between different phases, that may exist in practice.

(2) In the previous 1D-model very 'strict' microscopic mechanical boundary conditions are assumed to be present at the domain walls. This imposes strong restrictions on the values of the stresses and strains in the domains. *Here*, we will not use any local mechanical boundary conditions related to the domain walls. We argue that this is a justified assumption if one considers the domain walls to be regions of finite thickness in which all the stress, strain, and polarization gradients are confined, while in the domains no gradients are present. However, we have already argued that the (change of the) energy contribution of the domain walls can be neglected, thus the film consists of

domains with homogeneous stress and strain fields, only coupled by the macroscopic boundary conditions, which in essence impose dimensional constraints on the film, i.e. clamping. We will see that this assumption also allows for the possibility of different stress and strain states to exist in the domains at both sides of a domain wall, which was not the case in the 1D model.

(3) The electrical boundary conditions on the domain wall, as were used previously, relate the orientations and absolute values of the polarization on both sides of the domain wall. Fixed angles between the orientations were assumed, for example due to an uncharged 90° domain wall in the c/a domain phase. However, it is well known that this angle α is slightly less, depending on the short and long tetragonal lattice parameters a_T and c_T as $\alpha = 2a\tan(a_T/c_T)$, as follows from a simple geometric argument [8]. Leaving the domain wall angle α free makes it possible that the polarization vector length and orientation in differently oriented domains may vary under varying stress conditions due to an applied external electrical field. Therefore, we do not impose electrical boundary conditions on the domain walls.

In conclusion, the only condition imposed on the domain walls is that they are formed in such a way that the total energy of the film is minimized, but that the contribution of the domain wall energy to the total energy can be neglected. This condition applies to all types of domain walls, for example those between c and a domains, but also those separating c/a and c/b domain structures.

2.3.1 Free Energy of a Polydomain, Clamped (001)-Oriented Thin Film

The Gibbs energy of a bulk PZT ferroelectric is usually given by a sixth-order polynomial in the polarization components P_i and the internal mechanical stresses σ_{ij} [5],

$$\begin{aligned} G &= G_0 - \frac{1}{2}s_{klmn}\sigma_{kl}\sigma_{mn} - Q_{klmn}\sigma_{kl}P_mP_n \\ G_0 &= \alpha_1\left(P_1^2+P_2^2+P_3^2\right) + \alpha_{11}\left(P_1^4+P_2^4+P_3^4\right) + \alpha_{111}\left(P_1^6+P_2^6+P_3^6\right) \\ &\quad + \alpha_{12}\left(P_1^2P_2^2+P_3^2P_2^2+P_1^2P_3^2\right) + \alpha_{123}\left(P_1^2P_2^2P_3^2\right) \\ &\quad + \alpha_{112}\left(P_1^4\left(P_2^2+P_3^2\right) + P_2^4\left(P_1^2+P_3^2\right) + P_3^4\left(P_2^2+P_1^2\right)\right) \end{aligned} \tag{2.2}$$

$\alpha_1, \alpha_{kl}, \alpha_{klm}$ are the dielectric and higher order stiffness coefficients at constant stress. The temperature dependence of the properties are determined by that of the only temperature dependent parameter in the model, $\alpha_1 = (T - T_C)/2\varepsilon_0 C$, where T_C, C, and ε_0 are the bulk Curie-Weiss temperature, Curie-Weiss constant, and the vacuum permittivity, respectively. $s_{klmn} = s_{ij}$ are the elastic compliances at constant

polarization and $Q_{klmn} = Q_{ij}$ the electrostrictive constants. (The subindices i and j are used to denote the Voigt notation, which we will use from here on). The strains can be obtained from the thermodynamic relations $S_i = -\partial G/\partial\sigma_i$. For a clamped (001)-oriented thin film with an applied electrical field $\vec{E} = (0, 0, E)$ between the top and bottom electrode, the appropriate thermodynamic potential is the Helmholtz-free energy $F = G + \sum_{i=1}^{6} S_i\sigma_i - EP_3$ [9]. Eliminating the strains one obtains for domain x with isotropic properties (which can be for example a tetragonal c, a, or b domain with the long axis and polarization vector direction, respectively in the pseudocubic (001) (further-on denoted by the subindex 3), (100) (subindex 1), or (010) (subindex 2) directions) the energy density

$$\begin{aligned} F_x = {} & \alpha_1\left(P_{x1}^2 + P_{x2}^2 + P_{x3}^2\right) + \alpha_{11}\left(P_{x1}^4 + P_{x2}^4 + P_{x3}^4\right) + \alpha_{111}\left(P_{x1}^6 + P_{x2}^6 + P_{x3}^6\right) \\ & + \alpha_{12}\left(P_{x1}^2P_{x2}^2 + P_{x3}^2P_{x2}^2 + P_{x1}^2P_{x3}^2\right) + \alpha_{123}\left(P_{x1}^2P_{x2}^2P_{x3}^2\right) \\ & + \alpha_{112}\left(P_{x1}^4\left(P_{x2}^2 + P_{x3}^2\right) + P_{x2}^4\left(P_{x1}^2 + P_{x3}^2\right) + P_{x3}^4\left(P_{x2}^2 + P_{x1}^2\right)\right) \\ & + (s_{11}/2)\left(\sigma_{x1}^2 + \sigma_{x2}^2 + \sigma_{x3}^2\right) + s_{12}(\sigma_{x1}\sigma_{x2} + \sigma_{x1}\sigma_{x3} + \sigma_{x3}\sigma_{x2}) \\ & + (s_{44}/2)\left(\sigma_{x4}^2 + \sigma_{x5}^2 + \sigma_{x6}^2\right) - EP_{x3} \end{aligned} \tag{2.3}$$

We will use the index denoting the domain ($x = a, b, c, r$) as subindex as well as superindex, depending on the readability of the equation at hand. The total free energy of the film is then the sum of the energy contributions of the different domains and the domain wall energy

$$\langle F\rangle = \sum_x \phi_x F_x(P_{xi}, \sigma_{xi}, E) + F_{DW} \tag{2.4}$$

with ϕ_x the domain fraction of domain-type x. The clamped substrate condition imposes macroscopic mechanical boundary conditions in both in-plane directions

$$S_m = \langle S_1\rangle = \sum_x \phi_x S_{x1} = \langle S_2\rangle = \sum_x \phi_x S_{x2} \quad \langle S_6\rangle = \sum_x \phi_x S_{x6} = 0 \quad (2.5\text{a, b, c})$$

The last condition implies that there is no net shear in the film plane. There are no net forces acting on the upper surface, hence the corresponding average stresses (defined as above) are zero

$$\langle\sigma_3\rangle = \langle\sigma_4\rangle = \langle\sigma_5\rangle = 0 \tag{2.5d, e, f}$$

2.3.2 Application to a Tetragonal Polydomain Thin Film

In the following, we discuss in detail the case of the tetragonal composition at zero field. At finite fields the in-plane oriented polarization vectors may tilt slightly out-of-plane, which complicates the analytical study significantly, therefore we

assume here that there is no polarization tilt. The monodomain (c-phase) and polydomain phases (a/b, r phases) can be analyzed analogously. The total energy of a film in zero field with c, b, and a domains, arranged in substructures consisting of c/a, c/b, and a/b domain structures, after subtraction of the energy contribution of the domain walls, which is assumed to be constant, is

$$\langle F\rangle - F_{DW} = \langle F\rangle_{cba} = \phi_{ca}\langle F\rangle_{ca} + \phi_{cb}\langle F\rangle_{cb} + \phi_{ab}\langle F\rangle_{ab} \tag{2.6}$$

$\langle F\rangle_{ca}$ is the energy of a c/a domain structure with fraction ϕ_{ab} of the film volume and the other parameters defined analogously. After cycling the film to a large field ('poling' the film) one expects that the a/b substructure is removed and the film predominantly shows equal fractions of c/a and c/b domains. In this situation $\langle F\rangle_{ca} = \langle F\rangle_{cb}$. With $F_a = F_b$ due to symmetry, one obtains

$$\begin{aligned}\langle F\rangle_{cba} &= \phi_{ca}[\phi F_c + (1-\phi)F_a]_{ca} + \phi_{cb}[\phi F_c + (1-\phi)F_b]_{cb} \\ &= \phi F_c + (1-\phi)F_a\end{aligned} \tag{2.7}$$

The latter result is formally the same as for the 1D case. The difference is in the macroscopic boundary conditions (2.5a, b, c–2.5d, e, f), where the summation runs over the three possible domains. Note that this relation is independent of the assumed domain structure and could even describe a film which also contains a/b subdomain structures.

The 'strict microscopic boundary conditions', in combination with the macroscopic boundary conditions, impose very strict limitations on the stresses, namely $\sigma_3^c = \sigma_3^a = \sigma_4^c = \sigma_4^a = \sigma_5^c = \sigma_5^a = \sigma_6^c = \sigma_6^a = 0$ and $\sigma_1^c = \sigma_1^a$, $\sigma_2^c = \sigma_2^a$. Applying the strict conditions to the 2D problem one finds that $\sigma_1^c = \sigma_1^a = \sigma_1^b = \sigma_2^c = \sigma_2^a = \sigma_2^b \equiv \sigma$. In the 1D case, the result of the analysis is that $\left(\sigma_1^c = \sigma_1^a\right) \neq \left(\sigma_2^c = \sigma_2^a\right)$. Further on we will often use the 'strict electrical boundary conditions' $P_3^c = P_1^a = P$, in order to make analytical development possible. We note that only for zero field this is an exact solution, as is confirmed by the numerical study, hence all analytical results for zero field are still exact. However, we will *not* use the strict mechanical domain wall boundary conditions, but only the macroscopic boundary conditions. The macroscopic boundary conditions (2.5a, b) reduce to

$$S_m = \langle S_1\rangle = \langle S_2\rangle = \phi^{ca}\langle S_2\rangle^{ca} + \phi^{cb}\langle S_2\rangle^{cb} = \frac{1}{2}\left(\langle S_2\rangle^{ca} + \langle S_1\rangle^{ca}\right) \tag{2.8}$$

Here $\langle S_i\rangle^{ca} = \phi\langle S\rangle_i^c + (1-\phi)S_i^a$ is the average strain in the c/a domain structure in the in-plane directions $i = 1, 2$. Further use was made of the symmetry relations $\langle S_2\rangle^{cb} = \langle S_1\rangle^{ca}$ and $\langle S_1\rangle^{cb} = \langle S_2\rangle^{ca}$. From the boundary conditions (2.5c–f) it follows that $\phi\sigma_i^c + (1-\phi)\sigma_i^a = 0$ for $i = 3, 4, 5, 6$. Substituting the expressions for the strain, obtained from the thermodynamic relations, one arrives at the following expression for the c-domain fraction in the $c/b/a$ domain structure

$$\phi = \frac{[Q_{11} + Q_{12}]P^2 - 2S_m + (s_{11} + s_{12})\left(\sigma_1^a + \sigma_2^a\right)}{[Q_{11} - Q_{12}]P^2 - (s_{11} + s_{12})\left(\sigma_1^c + \sigma_2^c - \sigma_1^a - \sigma_2^a\right)} \tag{2.9a}$$

To make the connection with experimentally determined lattice parameters $a_{ix} = a_0\left(1 + S_i^x\right)$, (2.9a) can also be written as

$$\phi = \frac{a_{1a} + a_{2a} - 2a_s^*}{-a_{1c} + a_{1a} - a_{2c} + a_{2a}} \tag{2.9b}$$

Thus irrespective of the stress in the domains, the domain fraction can be obtained from the *measured* lattice parameters in the *c* and *a* domains. In the stress-free state $a_{1c} = a_{2c} = a_{2a} = a_{3a} = a_T$ and $a_{3c} = a_{1a} = c_T$ with a_T and c_T the bulk lattice parameters and (2.9b) reduces to

$$\phi = \frac{c_T + a_T - 2a_s^*}{c_T - a_T} \tag{2.9c}$$

(2.9a) is valid for arbitrary polarization and stress in the domains. Homogeneous stress conditions, $\sigma_1^c = \sigma_1^a = \sigma_2^c = \sigma_2^a \equiv \sigma$, apply if only the macroscopic boundary conditions are used and when there is no effect of the domain walls. One could consider the film as a strained membrane composed of connected smaller '*c*', '*a*', and '*b*' membranes, strained at the outer edge by the substrate. We will see that this condition also follows from numerical minimization of the energy, where we find $\sigma = 0$ for $E = 0$. We note that in practice the homogeneous stress condition may not necessarily apply, since local stress fields may arise from the dense domain wall structure, giving rise to inhomogeneous stress fields in the film. This is not discussed further here. With homogeneous stress (2.9a) becomes

$$\phi = \frac{[Q_{11} + Q_{12}]P^2 - 2S_m + 2(s_{11} + s_{12})\sigma}{[Q_{11} - Q_{12}]P^2} \tag{2.9d}$$

This result is different from that of the 1D case, which is a first consequence of considering the 2D domain structure.

The total energy (2.7) can now be written as

$$\begin{aligned}\langle F\rangle_{cba} = &\sum_{\mathrm{x=c,a}} \left\{\phi_x\left[\alpha_1 P_x^2 + \alpha_{11} P_x^4 + \alpha_{111} P_x^6\right]\right\} - \phi_c E P_3^c \\ &+ \phi_x\left[\frac{s_{11}}{2}\left(\sigma_{x1}^2 + \sigma_{x2}^2 + \sigma_{x3}^2\right) + s_{12}(\sigma_{x1}\sigma_{x2} + \sigma_{x1}\sigma_{x3} + \sigma_{x3}\sigma_{x2})\right. \\ &\left. + \frac{s_{44}}{2}\left(\sigma_{x4}^2 + \sigma_{x5}^2 + \sigma_{x6}^2\right)\right]\end{aligned} \tag{2.10}$$

Minimization with respect to the independent parameters σ_4^c, σ_5^c, and σ_6^c results in $\sigma_4^c = \sigma_5^c = \sigma_6^c = \sigma_4^a = \sigma_5^a = \sigma_6^a = 0$. Under homogeneous in-plane stress conditions the terms depending on σ_3^c also drop out. Further we use the strict polarization

conditions: (a) $P_3^c = P_1^a \equiv P$ (which is true for $E \approx 0$) and (b) all other polarization components equal zero. Hence there is no polarization rotation, thus the a and b domains do not develop a 3-component. We will show that the latter simplification leads to significant errors in the properties that depend on derivatives of the polarization and domain fraction with respect to the applied field, so that numerical analysis is required. Equation (2.10) becomes

$$\langle F\rangle_{cba} \approx \alpha_1 P^2 + \alpha_{11} P^4 + \alpha_{111} P^6 - \phi EP + (s_{11} + s_{12})\sigma^2 \tag{2.11}$$

Combining (2.9d) and (2.11) we find

$$\langle F\rangle_{cba} \approx \alpha_1 P^2 + \alpha_{11} P^4 + \alpha_{111} P^6 - QEP + \frac{SE}{P} - \frac{T_1 \sigma E}{P} + T_2 \sigma^2 \tag{2.12}$$

with $Q = (Q_{11} + Q_{12})/(Q_{11} - Q_{12})$, $S = 2S_m/(Q_{11} - Q_{12})$, $T_1 = 2(s_{11} + s_{12})/(Q_{11} - Q_{12})$ and $T_2 = (s_{11} + s_{12})$.

The (exact) zero-field solutions are found by minimization of (2.12) as

$$\sigma(0) = 0 \quad P^2(0) = P_s^2 = -\frac{\alpha_{11}}{3\alpha_{111}} + \left(\left(\frac{\alpha_{11}}{3\alpha_{111}}\right)^2 - \frac{\alpha_1}{3\alpha_{111}}\right)^{1/2} \tag{2.13}$$

The saturation polarization P_s value corresponds to the stress-free bulk value, P_s^{blk} [5]. The important conclusion is that in the 2D case the field-free domain structure resolves all stress in the film *in both in-plane* directions, which is the second difference with the 1D model. This also implies that for $E = 0$ the lattice parameters in all domains are equal to the bulk lattice parameters (see also (2.21) and the domain fraction is given by (2.9c) or (2.9d) with zero stress.

The measured (index f) remanent polarization of the film is

$$P_3^f(0) = \phi_0 P_s \tag{2.14}$$

where $(0) \equiv \phi_0$ is determined from (2.9d) with $\sigma = 0$ and $P = P_s$. Under the strict polarization condition one finds for finite fields by minimization of (2.12)

$$-QEP^2 + 2\alpha_1 P^3 + 4\alpha_{11} P^5 + 6\alpha_{111} P^7 = (S - T_1\sigma)E \tag{2.15a}$$

$$\sigma = \frac{T_1}{2PT_2} E = \frac{1}{(Q_{11} - Q_{12})P} E \tag{2.15b}$$

This set of equations determines the $P - E$ and $\sigma - E$ dependencies from which the film properties in the $c/b/a$ phase can be calculated.

2.3.3 Dielectric Properties of the Tetragonal (001) Polydomain Film

The measured dielectric constant for the film with top and bottom electrodes (under strict polarization conditions) is

$$\varepsilon_0 \varepsilon_{33}^f = \left(\frac{\partial P_3^f}{\partial E}\right)_{E=0} = \left(\frac{\partial \phi P}{\partial E}\right)_0 = \left(\frac{\partial \phi}{\partial E}\right)_0 P_s + \phi_0 \left(\frac{\partial P}{\partial E}\right)_0 \tag{2.16}$$

Thus, we need expressions for the field derivatives in the right-hand side. For further use we linearize (2.9d) as $\phi(S_m, E) = \phi_{0,0} + a_{\phi S} S_m + a_{\phi E} \mathrm{E}$. For zero field (hence zero stress) we have immediately

$$\phi_{0,0} = \frac{Q_{11} + Q_{12}}{Q_{11} - Q_{12}} = Q \quad a_{\phi S} = \frac{-2}{(Q_{11} - Q_{12}) P_s^2} \tag{2.17}$$

The values of these parameters are of the order $a_{\phi S} \approx -55$ and $\phi_{0,0} \approx 0.4{-}0.5$ for $x = 0.5{-}0.6$. Combining (2.15b) and (2.9d) a relation between electrical field and the domain fraction is obtained, from which follows

$$\left(\frac{\partial \phi}{\partial E}\right)_0 = \frac{4 S_m \left(\frac{\partial P}{\partial E}\right)_0}{(Q_{11} - Q_{12}) P_s^3} + \frac{2(s_{11} + s_{12})}{(Q_{11} - Q_{12})^2 P_s^3} \tag{2.18}$$

Hence $a_{\phi E} = (\partial \phi / \partial E)_{0, S_m = 0} = 2(s_{11} + s_{12}) / (Q_{11} - Q_{12})^2 P_s^3$, which is of the order of 0.05/(100 kV/cm) (100 kV/cm corresponds to the electrical field range used in thin film applications), irrespective of composition. Values for the linearization parameters are given in Table 2.2, together with values obtained from the numerical calculations in Sect. 2.4. The analytical results for $\phi_{0,0}$ and $a_{\phi S}$ are equal to the numerically obtained values, while the analytical value of $a_{\phi E}$ is slightly less than found numerically. We will see further on that this is a consequence of the polarization assumption (b) in the analytical model, that the in-plane oriented domains do not couple to the external field.

Table 2.2 Linearized parameters for the domain fraction and polarization

	$\phi_{0,0}$ [b]	$a_{\phi S}$ [b]	$a_{\phi E}$ [b] (m/V)	$\varepsilon_{33}^c/\varepsilon_0$ [c]	$\varepsilon_{13}^c/\varepsilon_0$	$\varepsilon_{33}^a/\varepsilon_0$	$\varepsilon_{13}^a/\varepsilon_0$
PZT50/50	0.36 [a] (0.36) [a]	−56 (−56)	5.4×10^{-9} (8.4×10^{-9})	(−113)	(0)	(1706)	(305)
PZT40/60	0.47 (0.47)	−55 (−55)	5.1×10^{-9} (6.6×10^{-9})	(−17)	(0)	(497)	(186)

[a] Numerically obtained values in brackets, analytical values without brackets

[b] Linearized c-domain fraction $\phi = \phi_{0,0} + a_{\phi S} S_m + a_{\phi E}$

[c] $\varepsilon_{i3}^x/\varepsilon_0 = \left(\partial P_i^x / \partial E\right)_0 / \varepsilon_0$

The derivative $(\partial P/\partial E)_0$ follows from (2.15a)

$$\left(\frac{\partial P}{\partial E}\right)_{E=0} = \left(\frac{Q_{11}+Q_{12}}{Q_{11}-Q_{12}} + \frac{2S_m}{(Q_{11}-Q_{12})P_s^2}\right)\varepsilon_0\varepsilon_{33}^* \equiv \varepsilon_0\varepsilon^{ca} \tag{2.19}$$

Here $\varepsilon_0\varepsilon_{33}^* = \left(6\alpha_1 + 20\alpha_{11}P_s^2 + 42\alpha_{111}P_s^4\right)^{-1}$ is a dielectric constant of similar functional form as that of an unstrained, monodomain, tetragonal PZT $\varepsilon_0\varepsilon_{33}^{blk} = \left(2\alpha_1 + 12\alpha_{11}P_s^2 + 30\alpha_{111}P_s^4\right)^{-1}$ [5]. Since $\varepsilon_{33}^* > 0$ the gradient $(\partial P/\partial E)_0$ varies linearly with the strain and is even negative for $S_m < -P_s^2(Q_{11}+Q_{12})/2$, implying that the polarization in all domains decreases with increasing field in the strain range, $S_m = \left[P_s^2 Q_{12}, -P_s^2(Q_{11}+Q_{12})/2\right]$. This is again a consequence of the strict polarization conditions. Now we drop the approximation of the strict polarization conditions. In that case, the second term in (2.16) is to be replaced with a fraction weighted average of the dielectric constants of all domains

$$\begin{aligned}\varepsilon_0\varepsilon_{33}^f &= \left(\frac{\partial P_3^f}{\partial E}\right)_{E=0} = \left(\frac{\partial\left(\phi P_3^c + (1-\phi)P_3^a\right)}{\partial E}\right)_0 \\ &= \left(\frac{\partial\phi}{\partial E}\right)_0 P_s + \phi_0\left(\frac{\partial P_3^c}{\partial E}\right)_0 + (1-\phi_0)\left(\frac{\partial P_3^a}{\partial E}\right)_0 \qquad (2.20a)\\ &\approx a_{\phi E}P_s + \varepsilon_0\varepsilon_{33}^a + \varepsilon_0\left(\varepsilon_{33}^c - \varepsilon_{33}^a\right)\left[\phi_{0,0} + a_{\phi S}S_m\right] \qquad (2.20b)\end{aligned}$$

From the numerical study, in which these approximations are not used, one finds (for the 40/60 composition) that $\left(\partial P_3^c/\partial E\right)_0/\varepsilon_0 \equiv \varepsilon_{33}^c/\varepsilon_0 \approx -17$, $\left(\partial P_1^c/\partial E\right)_0/\varepsilon_0 \equiv \varepsilon_{13}^c/\varepsilon_0 \approx 0$, while $\left(\partial P_3^{a,b}/\partial E\right)_0/\varepsilon_0 \equiv \varepsilon_{33}^a/\varepsilon_0 \approx 497$, and $\left(\partial P_1^{a,b}/\partial E\right)_0/\varepsilon_0 \equiv \varepsilon_{13}^a/\varepsilon_0 \approx 186$ for all S_m. Naively, one would expect that the $\partial P/\partial E$ dependence would arise from the *c*-domains and this is also the result of the polarization approximations (a) and (b) leading to (2.16). However, from (2.20a, b) it is seen that this dependence is nearly fully due to the out-of-plane rotation of the polarization vector of the *a*-domains under influence of the applied field. The difference in field dependence of the various components of the polarization in different domains under the assumptions leading up to (2.16) and (2.20a, b) has a profound effect on $\varepsilon_0\varepsilon_{33}^f$ and one needs the numerical analysis to obtain values for $\left(\partial P_i^x/\partial E\right)_0$. The dependence on the change of the domain fraction with applied field is still the same as in (2.16). We note that this term depends on the measurement frequency in *ac*-measurements due to the domain wall motion, making it sensitive to domain wall pinning. The other terms arise from the static *P*-*E* loop and depend on the strain.

2.3.4 Lattice Parameters of the Tetragonal (001) Polydomain Film

The lattice strains as function of electric field are obtained (using the relaxed polarization conditions) as

$$\begin{aligned}
S_1^c &= S_2^c = (s_{11}+s_{12})\sigma + Q_{12}P_{3c}^2 \approx \frac{(s_{11}+s_{12})}{(Q_{11}-Q_{12})P_s}E + Q_{12}P_s^2 + 2Q_{12}\varepsilon_{13}^c P_s E \\
S_1^a &= (s_{11}+s_{12})\sigma + Q_{11}P_{1a}^2 + Q_{12}P_{3a}^2 \approx \frac{(s_{11}+s_{12})}{(Q_{11}-Q_{12})P_s}E + Q_{11}P_s^2 + 2Q_{11}\varepsilon_{13}^a P_s E \\
S_2^a &= (s_{11}+s_{12})\sigma + Q_{12}P_{1a}^2 + Q_{12}P_{3a}^2 \approx \frac{(s_{11}+s_{12})}{(Q_{11}-Q_{12})P_s}E + Q_{12}P_s^2 + 2Q_{12}\varepsilon_{13}^a P_s E \\
S_3^c &= 2s_{12}\sigma + Q_{11}P_{3c}^2 \approx \frac{2s_{12}}{(Q_{11}-Q_{12})P_s}E + Q_{11}P_s^2 + 2Q_{11}\varepsilon_{33}^c P_s E \\
S_3^a &= 2s_{12}\sigma + Q_{12}P_{1a}^2 + Q_{11}P_{3a}^2 \approx \frac{2s_{12}}{(Q_{11}-Q_{12})P_s}E + Q_{12}P_s^2 + 2Q_{12}\varepsilon_{13}^a P_s E \\
S_4^c &= S_5^c = S_6^c = S_4^a = S_5^a = S_6^a = 0
\end{aligned} \tag{2.21}$$

The lattice parameters follow from $a_i^x = a_0\left(1+S_i^x\right)$. Because $\varepsilon_{13}^c/\varepsilon_0 \approx 0$ the short axes of the *c*-domain unit cells only increase with the field due to the stress term, while the long axis decreases in length due to both the stress and the piezoelectric effect ($\varepsilon_{33}^c < 0$). Because ε_{33}^c is very small the length change is dominated by the stress. The long, in-plane axis of the *a*-domain is elongated by the stress and the piezoelectric effect. The *a*-domain short axes respond differently to the stress, but both shorten by the piezoelectric effect. Under the strict polarization conditions similar relations are found, but with $\varepsilon_{ij}^x = \varepsilon^{ca}$, from (2.19) and $P_{ix} = P_s$, clearly a different applied field dependence of the lattice parameters is found.

2.3.5 Piezoelectric Properties of the Tetragonal, Polydomain (001) Film

The average out-of-plane strain is given by $\langle S\rangle_3 = \phi S_3^c + (1-)S_3^a$, so that the effective piezoelectric parameter d_{33}^f at zero field, with the polarization approximations, is

$$d_{33}^f = \left(\frac{\partial\langle S_3\rangle}{\partial E}\right)_o^\sigma = \left(\frac{\partial\phi}{\partial E}\right)_0 (Q_{11}-Q_{12})P_s^2 + \frac{2s_{12}}{(Q_{11}-Q_{12})P_s} \tag{2.22a}$$

Dropping these approximations an extra term arises due to the piezoelectric effect

$$d_{33}^{f} \approx \left(\frac{\partial \phi}{\partial E}\right)_0 (Q_{11} - Q_{12})P_s^2 + \left[\phi_0 Q_{11}\varepsilon_{33}^{c} + (1-\phi_0)Q_{12}\varepsilon_{13}^{a}\right]2P_s + \frac{2s_{12}}{(Q_{11}-Q_{12})P_s} \tag{2.22b}$$

With $d_{33}^{c} \equiv 2Q_{11}\varepsilon_{33}^{c}P_s$, $d_{31}^{a} \equiv 2Q_{12}\varepsilon_{13}^{a}P_s$ the relevant piezoelectric coefficient of the c and a-domains, this can also be written as

$$d_{33}^{f} = a_{\phi E}(c_T - a_T) + \left(\phi_0 d_{33}^{c} + (1-\phi_0)d_{31}^{a}\right) + \frac{2s_{12}P_s}{(c_T - a_T)} \tag{2.22c}$$

The first right-hand term in (2.22), due to domain wall motion (which we name d_{33}^{DW}), is a measure of the change of the weighting of the out-of-plane lattice parameters. The second term in (2.22b, 2.22c) and missing in (2.22a), is a weighted average of the piezoelectric effects in the c and a-domains (named d_{33}^{PE}). The last, elastic term, d_{33}^{elas}, arises from the field dependence of the lattice parameters through the changing stress and is negative. The signs of both d_{33}^{c} and d_{31}^{a} are negative, thus only the domain wall motion gives rise to a positive piezoelectric constant, but its effect is counteracted by the intrinsic piezoelectric effect and stress buildup in the film. The second and third term do not depend on (frequency dependent) domain wall motion, whereas the first term does. All other average strains and strain derivatives with respect to the field are zero, thus the other piezoelectric coefficients are $d_{ij} = 0$.

The in-plane stress components are given by (2.15b) $\sigma_1^c = \sigma_1^a = \sigma_2^c = \sigma_2^a = \sigma = E/(Q_{11} - Q_{12})P_s$. All other stress components are zero. Thus, the nonzero piezoelectric coefficients e_{3i} are obtained from (2.15b) as

$$e_{31} = e_{32} = -\left(\frac{\partial \sigma_1}{\partial E}\right)_0^S = \frac{-1}{(Q_{11}-Q_{12})P_s} \tag{2.23}$$

There is no direct dependence on the domain fraction. Further e_{31} is not dependent on the value of the strain either, only on intrinsic piezoelectric and elastic properties. The usual expression for e_{31} of a clamped thin film is $e_{31} = d_{31}/(s_{11} + s_{12})$ [13]. The difference between these expression arises from the fact that (2.23) is the result of considering in detail the domain distribution of the film and expressing all film parameters in terms of microscopic properties, while the usual clamped film result is derived from a model not taking domain formation into account and in principle using averaged properties.

2.4 Numerical Analysis

The numerical analysis is performed for the $c/bc^*/ac^*$—phase with the two free energy functions for the c and a domain coupled by the domain fraction, used as

free parameter, and for $\sigma^x_{3,4,5,6} = 0$. Further all polarization vector components of the c and a domain and in-plane stresses were taken as independent-free parameters. The energy minimization of (2.7) gives solutions for the polarization vector components and ϕ, and shows that all in-plane stress components are always equal, as was also found analytically. The polydomain phase goes over into the single domain c-phase for $\phi = 1$, into the polydomain ac^*/bc^*-phase at $\phi = 0$ and into the p—phase, when the polarization components are equal to 0. Due to symmetry only one free energy function is needed to describe the rhombohedral phase, with $\sigma^r_{3,4,5,6} = 0$ (which follows from analytical minimization), but with $\sigma^r_1 = \sigma^r_2$ and the polarization vector components as free parameters. This phase goes over into the c-phase for $P_1 = P_2 = 0$. For all temperature, strain and field values the energy of the $c^*/bc^*/ac^*$ and the r-phase is calculated. The proper phase is that with the lowest free energy, for which the domain properties are obtained. The film properties are calculated as

$$\varepsilon^f_{33} = \frac{(\langle P_3\rangle(\delta E) - \langle P_3\rangle(0))}{\delta E} \tag{2.24a}$$

$$d^f_{33} = \frac{(\langle S_3\rangle(\delta E) - \langle S\rangle(0))}{\delta E} \tag{2.24b}$$

$$e^f_{31} = -\frac{(\sigma_1(\delta E) - \sigma_1(0))}{\delta E} \tag{2.24c}$$

with $\delta E = 1$ kV/cm.

2.4.1 Numerical Results

Here we compare the results for the rhombohedral compositions PZT60/40, the PZT50/50 composition close to the MPB, and the tetragonal composition PZT40/60. Figure 2.2 gives the $T - S_m$ temperature strain phase diagrams at zero field.

Contrary to the earlier 1D model, which showed several additional phases, very simple phase diagrams are found with only c, $c/b/a$, and a/b phases and the paraelectric phase at high temperatures. The $c - c/b/a$ phase boundaries in the $T - S_m$ diagram of the tetragonal as well as the rhombohedral compositions are defined by $\phi_0 = 1$ in (2.9d) resulting in the relation $S_m = Q_{12}P_s^2$, while the $c/b/a - a/b$ phase

Fig. 2.2 Temperature-Strain ($T - S_m$) phase diagrams at zero field (**a**–**c**) and Electrical Field ▶ Strain ($\boldsymbol{E} - \boldsymbol{S_m}$) phase diagrams at room temperature (**d**–**f**) of PZT60/40 (**a**, **d**), PZT50/50 (**b**, **e**), and PZT40/60 (**c**, **f**). The transition in the ($\boldsymbol{E} - \boldsymbol{S_m}$) diagram of the $\boldsymbol{a/b}$ phase (*orange*) to the $\boldsymbol{ac^*/bc^*}$ (*red*) and from the $\boldsymbol{c/b/a}$ (*blue*) to $\boldsymbol{c/bc^*/ac^*}$ (*green*) occurs at $E = 0$, but is (arbitrarily) drawn for a field value of $P^{a,b}_3 = 0.01P^{a,b}_1$, to clarify this phase transition. The maximum applied field corresponds to a voltage of 20 V over a 1 μm ferroelectric layer

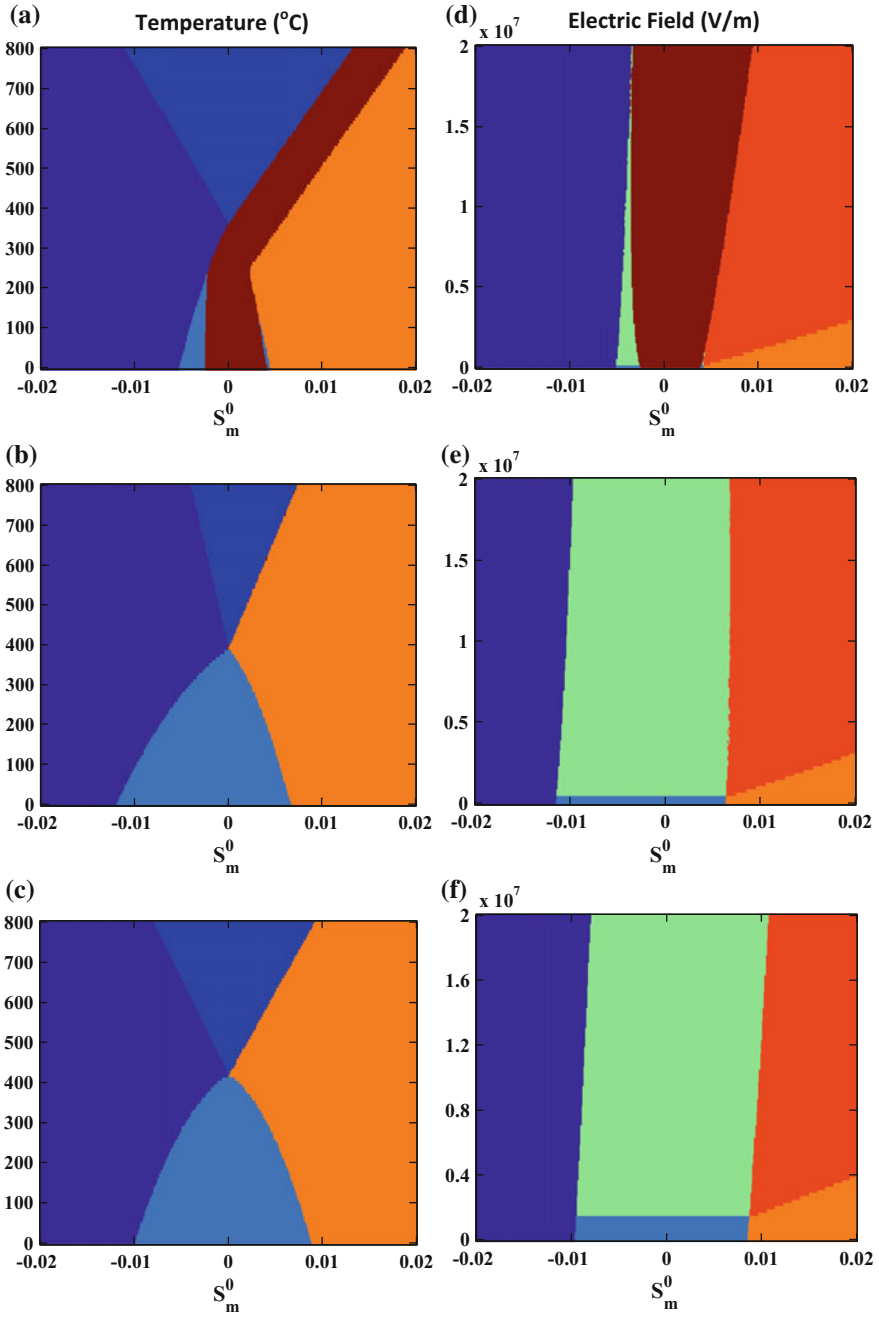
(a)
Temperature (°C)
(d)
x 10^7
Electric Field (V/m)
(b)
(e)
(c)
(f)
S^0_m

boundary is found for $\phi_0 = 0$ as $S_m = \frac{1}{2}(Q_{11} + Q_{12})P_s^2$. For PZT60/40, the r-phase largely replaces the $c/b/a$ phase. The latter only occurs at lower temperatures close to the phase boundaries with the c and a/b phases, forming a transition phase between the r-phase and the c and a/b phases. It is seen that in the experimentally accessible range of substrate induced strains, the domain structure tends to be in the $c/b/a$ phase for $x \geq 0.5$ and in the r-phase for smaller x. Thus, the model predicts no other phases in films on usual substrates, than are present in the bulk phase. The $E - S_m$ field-strain phase diagrams at room temperature show that the applied field poses a relatively small force on the system, since the phase boundaries between the c, $c/b/a$, and a/b phases are nearly vertical, except for the transition between the a/b and r phases, indicating that under the influence of the field the polarization rotates rapidly out-of-plane. Further the polarization vector of the in-plane oriented a and b domains quickly develop an out-of-plane component with increasing field, changing the $(c/)b/a$ domain structure into the $(c/)bc^*/ac^*$ structure. In Fig. 2.3, the in-plane stress and the c-domain fraction are given for zero and large field, versus the substrate strain. The 2D model resolves all stress in the $c/b/a$ phase by changing the domain fraction, as was also found analytically. The (absolute) stress rapidly increases when ϕ reaches its limits 0 and 1 in the a/b phase, respectively c phase. In the r-phase the stress is mostly nonzero, but the polarization rotation is used to minimize the stress and thus the elastic energy. For finite fields the stress increases, reducing the energy gain by the electric field terms in (3). The change in stress with field is largest in the $c/b/a$ and r phases. The numerical analysis shows that the domain fraction ϕ in the $c/b/a$ phase varies linearly with strain and field, in good accordance with (2.9d, 2.17). The stress scales in good approximation with applied field according to (2.15b) for the tetragonal compositions.

The components of the polarization in the various domains for zero and large field as well as the lattice parameters are shown in Fig. 2.4 as function of substrate induced strain. For $x \geq 0.5$, the lattice parameters and the polarization components in the $c/b/a$-phase at zero field do not depend on the strain S_m because the stress is

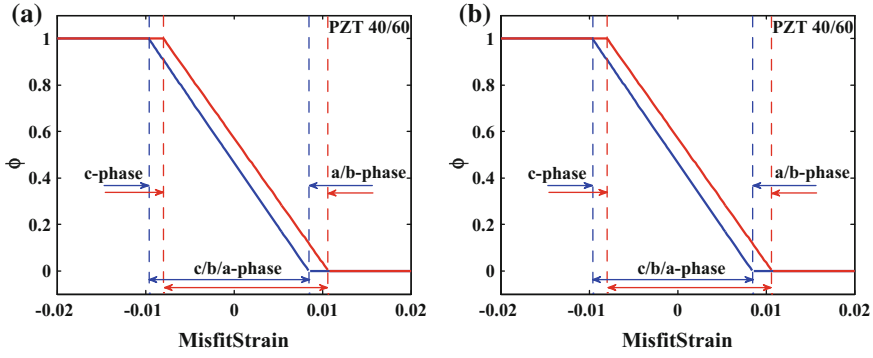

Fig. 2.3 c-domain fraction ϕ for the tetragonal PZT40/60 composition (**a**) and in-plane stress σ for the PZT60/40, 50/50 and 40/60 compositions (**b**) as function of substrate induced strain at applied field $E = 0$ (*blue*) and $E = 2 \times 10^7$ V/m (*red*)

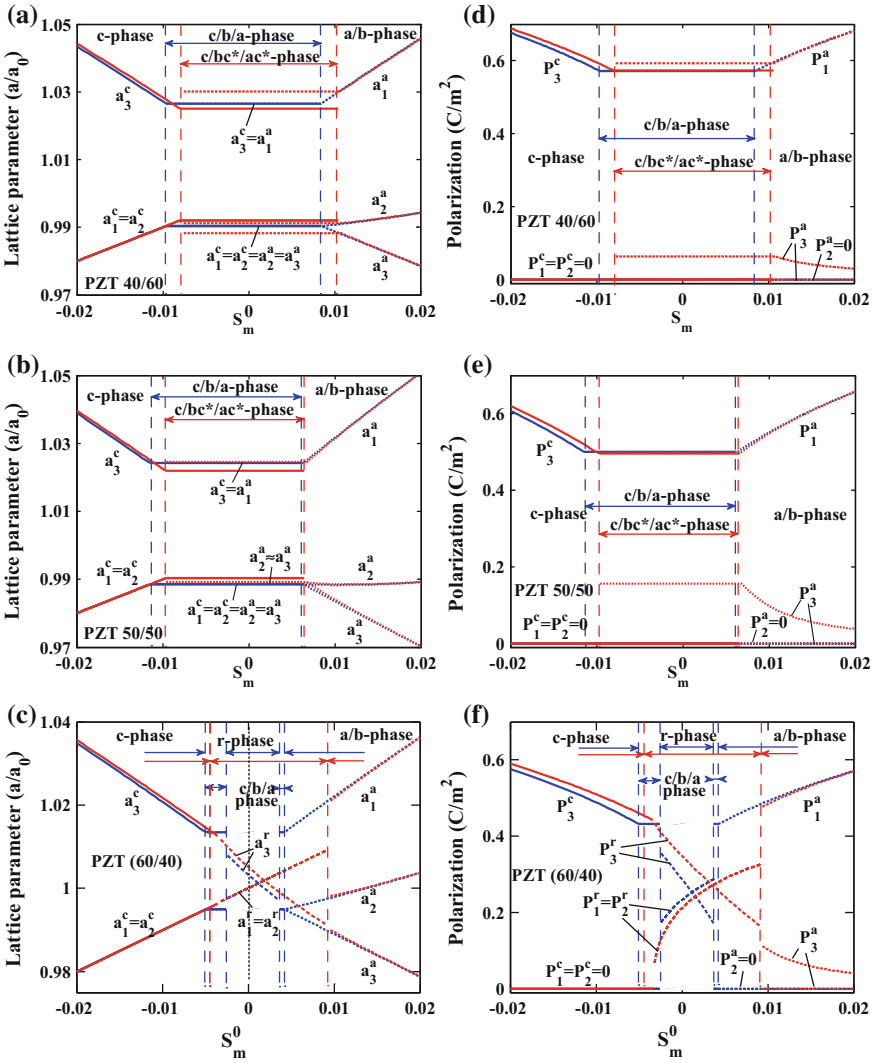

Fig. 2.4 Lattice parameters (**a–c**) and polarization components (**d–f**) as function of substrate induced strain at applied fields $E = 0$ (*blue*) and $E = 2 \times 10^7$ V/m (*red*)

zero, as predicted by (2.21). By shifting the domain walls the elastic energy can be minimized for given field and strain. With increasing field the stress increases, but also the polarization vector components change. The energy minimization determines which factors are most important in the resulting strains. It is seen that the long axis of the *c*-domain decreases with field, while the short axes increase. The change in lattice parameters can be interpreted with the relations (2.21), showing the role of the piezoelectric effect and the field induced stress. Figure 2.4e, f clearly

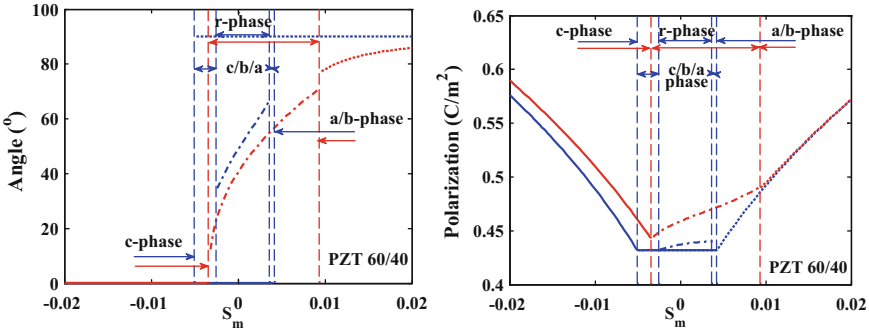

Fig. 2.5 Polarization extension and rotation in the *r*-phase versus strain at $E = 0$ (*blue*) and $E = 2 \times 10^7$ V/m (*red*)

show the significant out-of-plane rotation of the *a*-domain polarization vector under an applied field. This demonstrates that the strict polarization conditions (the polarization vectors in the various tetragonal domains have the same length and do not rotate under the applied field) are indeed very strong restrictions, which in a real film are likely not to hold. It is also observed that the *c*-domain polarization hardly changes in magnitude under applied field. Table 2.2 gives the strain and field dependences of the linearized expression for domain fraction and polarization components in the $c/b/a$ phase.

In the *r*-domain polarization rotation is the mechanism to adapt to varying conditions, which can be visualized better by writing the polarization vector as $\vec{P} = P_s(\sin\theta, \sin\theta, \cos\theta)$ with θ the angle of the polarization vector with length P_s and with the film normal. From Fig. 2.5 it is seen that the polarization in the *r*-phase rotates under the influence of the substrate strain, but that the polarization value is fairly constant. Also under applied field polarization rotation dominates the change in the polarization components, while P_s increases only in the order of a few percent under large fields. Further the polarization direction jumps abruptly at the phase boundaries, whereas the polarization length varies (nearly) continuously.

The film dielectric constant is shown in Fig. 2.6a. For the $c/b/a$, phase of the PZT50/50 and PZT40/60 the $\varepsilon_{33}^f/\varepsilon_0$ increases linearly with the strain, which is due to the last term in (2.20b). Using the linearized expression it is found that the first term due to domain wall motion is 475 for PZT50/50 and 425 for PZT40/60, respectively, while the second strain dependent term is equal to 1051 (281) for $S_m = 0$. Thus, the domain wall motion gives a significant, constant contribution to the dielectric constant. This also explains the abrupt drop in ε_{33}^f at the $c/b/a$ phase boundaries, when the domain wall contribution suddenly drops to zero. Equation (2.20b) indicates that the polarization change in the *c*-domains is so small that the main intrinsic contribution to ε_{33}^f arises from the *a*-domains. In the case of the *r*-domain we can write the dielectric constant in terms of polarization rotation and extension, $\varepsilon_0\varepsilon_{33}^f = (\partial P_3/\partial E)_0 = (\partial P_s/\partial E)_0\cos\theta_0 - P_s\sin\theta_0(\partial\theta/\partial E)_0$. From

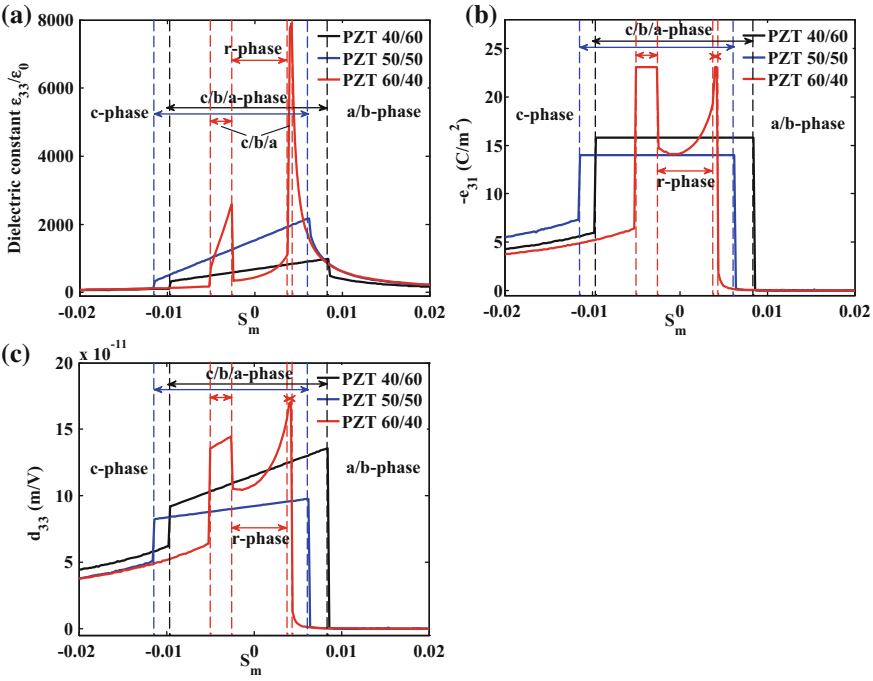

Fig. 2.6 Room temperature relative dielectric constant $\varepsilon_{33}^f/\varepsilon_0$ (**a**) Piezoelectric coefficients d_{33}^f (**b**) and e_{31}^f (**c**) at zero field obtained from the numerical analysis

numerical analysis, it can be shown that the ratio of the contributions of polarization rotation and extension is $\varepsilon_{33}^{\text{rot}}/\varepsilon_{33}^{\text{ext}} = 3.2$ for $S_m = 0$, thus $\varepsilon_0\varepsilon_{33}^f$ is dominated by polarization rotation.

The piezoelectric coefficient d_{33}^f of the tetragonal compositions, plotted in Fig. 2.4b, can most easily be interpreted in terms of (2.22b). Using the linearized forms of polarization and domain fraction, one finds for the 'domain wall motion' term d_{33}^{DW} = 299, and 237 pm/V for PZT50/50 and 40/60, respectively. The second, 'piezoelectric' term is $d_{33}^{PE} = -114$ (−38 pm/V), and the third, 'elastic' term $d_{33}^{\text{elas}} = -104$ (−89 pm/V), resulting in d_{33}^f = 81 and 110 pm/V for the two materials, in good accordance with the numerical values. The substrate strain dependence is solely due to the term d_{33}^{PE}, which is always negative because the polarization P_3^c in the c-domain decreases with field (thus $\varepsilon_{33}^c < 0$), while that in the a-domain, P_1^a increases ($\varepsilon_{13}^a > 0$). Again, we see that the sharp drop of d_{33}^f at the $c/b/a$ phase boundaries is due to the disappearance of the field sensitive domain fraction. For the r-domain

$$d_{33}^{f} = 2s_{12}(\partial\sigma/\partial E)_0 + 2P_{s0}(\partial P_s/\partial E)_0\left(Q_{11}\cos^2\theta_0 + Q_{12}\sin^2\theta_0\right) - (\partial\theta/\partial E)_0 P_{s0}^2(Q_{11} - Q_{12})\sin 2\theta_0 \tag{2.25}$$

with P_{s0} and θ_0 the polarization length and angle at zero field and given strain. The first term is due to elastic effects ($d_{33}^{\text{elas}} = -84$ pm/V for $S_m = E = 0$), while the second ($d_{33}^{\text{ext}} = 16$ pm/V) and third term ($d_{33}^{\text{rot}} = 149$ pm/V) are due to polarization extension and rotation, respectively. Thus, the piezoelectric effect is dominated by polarization rotation, while the polarization extension gives a small contribution ($d_{33}^{\text{rot}}/d_{33}^{\text{ext}} = 9.3$). The stress term causes a large opposing effect. The numerical results for the piezoelectric coefficient e_{31}^{f} of the tetragonal compositions are well described by (2.23).

2.5 Conclusions and Outlook

The model discussed in this chapter describes the properties of polydomain (001)-oriented PZT thin films, assuming the presence of three different domains in the tetragonal phase. Further, the domain walls are assumed not to impose boundary conditions on the stresses and polarizations in the domains. These assumptions are the main differences with an earlier model in the literature. It is believed that the present model gives a more realistic description. The new assumptions give the system more degrees of freedom to find an energy minimum.

The properties of the film were studied analytically as well as numerically. It is found that for the strain values induced by practically used substrates

(a) the tetragonal PZT compositions are always in the polydomain tetragonal $c/b/a$-phase, while the rhombohedral compositions are in the polydomain r-phase. The near MPB 50/50 composition is found to be in the $c/b/a$-phase.
(b) In the $c/b/a$-phase, the stresses in both in-plane directions are equal at finite applied field values, and zero at zero field. The elastic energy in the film is therefore zero at zero field and the film is not strained.
(c) The analysis allows to decompose the dielectric and piezoelectric properties. In the $c/b/a$-phase the dielectric constant of the film, ε_{33}^{f}, is due to domain wall motion and the rotation of the polarization vector of the in-plane domains, whereas the c-domains do not contribute. The piezoelectric constant of the film, d_{33}^{f}, is due to domain wall motion, the piezoelectric effect of the in-plane domains (no effect from the c-domains) and elastic effects depending on the domain fractions. The piezoelectric constant e_{31}^{f} is not dependent on the domain fractions, but only on the electrostrictive coefficients.

(d) The numerical study shows that in the *r*-phase the polarization rotates under the influence of substrate strain and applied field, whereas the polarization extension is fairly small. Hence the stress energy in the film is reduced by changing the rhombohedral angles of the unit cell.

Acknowledgments This work was supported by NanoNextNL, a micro and nanotechnology consortium of the Government of the Netherlands and 130 partners. This research was carried out under the project number M62.3.10404 in the framework of the Research Program of the Materials innovation institute (M2i) (www.m2i.nl).

References

1. M. Bayraktar, A. Chopra, F. Bijkerk, G. Rijnders, Appl. Phys. Lett. **105**, 132904 (2014)
2. P.K. Davies, H. Wu, A.Y. Borisevich, I.E. Molodetsky, L. Farber, Ann. Rev. Mat. Res. **38**, 369 (2008)
3. M. Dekkers, M.D. Nguyen, R. Steenwelle, P.M. te Riele, D.H.A. Blank, G. Rijnders, Appl. Phys. Lett. **95**, 012902 (2009)
4. H.-U. Habermaier, Mater. Today **10**, 34 (2007)
5. M.J. Haun, E. Furman, S.J. Jang, L.E. Cross, Ferroelectrics **99**, 13 (1989)
6. E.P. Houwman, M.D. Nguyen, M. Dekkers, G. Rijnders, Sci. Techn. Adv. Mater. **14**, 045006 (2013)
7. E.P. Houwman, K. Vergeer, G. Koster, G. Rijnders. unpublished
8. C. Kittel, Sol. State Comm. **10**, 119 (1972)
9. V.G. Koukhar, N.A. Pertsev, R. Waser, Phys. Rev. B **64**, 214103 (2001)
10. V.G. Kukhar, N.A. Pertsev, H. Kohlstedt, R. Waser, Phys. Rev. B **73**, 214103 (2006)
11. Li, Y.L., Hu, S.Y., Liu, Z.K., Chen, L.Q., Appl. Phys. Lett. **78**, 3878 (2001)
12. Y.L. Li, S.Y. Hu, Z.K. Liu, L.Q. Chen, Acta Mater. **50**, 395 (2002)
13. P. Muralt, A. Kholkin, M. Kohli, T. Maeder, Sens. Actuators, A **53**, 397–403 (1996)
14. N.A. Pertsev, V.G. Koukhar, Phys. Rev. Lett. **84**, 3722 (2000)
15. Ramesh, R., Current Sci. **105** (2013)
16. A.L. Roitburd, Phys. Stat. Sol. (a) **37**, 329 (1976)
17. A.K. Tagantsev, L.E. Cross, J. Fousek, *Domains in Ferroic Crystals and Thin Films* (Springer, New York, 2010). ISBN 978-1-4419-1516-3
18. X. Wan, E.P. Houwman, R. Steenwelle, R. van Schaijk, M.D. Nguyen, M. Dekkers, G. Rijnders, Appl. Phys. Lett. **104**, 092902 (2014)
19. P. Zubko, S. Gariglio, M. Gabay, P. Ghosez, J.-M. Triscone, Ann. Rev. Cond. Matt. Phys. **2**, 141 (2011)